A&A 476, 1401–1409 (2007)
DOI: 10.1051/0004-6361:20078436

Astronomy & Astrophysics

Accurate early positions for *Swift* GRBs: enhancing X-ray positions with UVOT astrometry

M. R. Goad[1], L. G. Tyler[1], A. P. Beardmore[1], P. A. Evans[1], S. R. Rosen[1,3], J. P. Osborne[1], R. L. C. Starling[1], F. E. Marshall[2], V. Yershov[3], D. N. Burrows[4], N. Gehrels[2], P. W. A. Roming[4], A. Moretti[5], M. Capalbi[6], J. E. Hill[7], J. Kennea[4], S. Koch[4], and D. Vanden Berk[4]

[1] Department of Physics and Astronomy, University of Leicester, LE1 7RH, UK
e-mail: mrg@star.le.ac.uk
[2] NASA Goddard Space Flight Center, Greenbelt, MD 20771, USA
[3] Mullard Space Science Laboratory, Department of Space and Climate Physics, University College London, Holmbury St. Mary, Dorking, Surrey, RH5 6NT, UK
[4] Pennsylvania State University, University Park, PA 16802, USA
[5] INAF-Osservatorio Astronomica di Brera, via Bianchi 46, 23807 Merate (Lc), Italy
[6] ASI Science Data Center, via Galileo Galilei, 00044 Frascati, Italy
[7] Universities Space Research Association, 10211 Wincopin Circle, Suite 500, Columbia, MD 21044-3432, USA

Received 7 August 2007 / Accepted 13 October 2007

ABSTRACT

The *Swift* Gamma Ray Burst satellite routinely provides prompt positions for GRBs and their afterglows on timescales of a few hundred seconds. However, with a pointing accuracy of only a few arcminutes, and a systematic uncertainty on the star-tracker solutions to the World Coordinate System of 3–4 arcsec, the precision of the early XRT positions is limited to 3–4 arcsec at best. This is significant because operationally, the XRT detects >95% of all GRBs, while the UVOT detects only the optically brightest bursts, ~30% of all bursts detected by BAT; thus early and accurate XRT positions are important because for the majority of bursts they provide the best available information for the initial ground-based follow-up campaigns. Here we describe an autonomous way of producing more accurate prompt XRT positions for GRBs and their afterglows, based on UVOT astrometry and a detailed mapping between the XRT and UVOT detectors. The latter significantly reduces the dominant systematic error – the star-tracker solution to the World Coordinate System. This technique, which is limited to times when there is significant overlap between UVOT and XRT PC-mode data, provides a factor of 2 improvement in the localisation of XRT refined positions on timescales of less than a few hours. Furthermore, the accuracy achieved is superior to astrometrically corrected XRT PC mode images at early times (for up to 24 h), for the majority of bursts, and is comparable to the accuracy achieved by astrometrically corrected X-ray positions based on deep XRT PC-mode imaging at later times.

Key words. gamma ray: bursts – astrometry

1. Introduction

Since its launch in November 2004, the *Swift* Gamma-Ray Burst Explorer (Gehrels et al. 2004) has been routinely observing the prompt gamma-ray and early afterglow emission of Gamma-Ray Bursts (GRBs) in the astrophysically important minutes to hours timescale after the onset of the burst.

The *Swift* spacecraft carries 3 co-aligned intruments, the Burst Alert Telescope (herefter BAT, Barthelmy et al. 2004, 2005), the X-ray Telescope (hereafter XRT, Burrows et al. 2004, 2005) and the UltraViolet and Optical Telescope (hereafter UVOT, Roming et al. 2005). The BAT is a coded mask imager, comprised of 32 768 Cadmium Zinc Telluride (CdZnTe) detectors above which are randomly located 52 000 (5×5×1 mm) lead tiles. The BAT has a field of view of 1.4 sr (half-coded), capable of imaging in the range 20–150 keV, with a spatial resolution of 17 arcmin and a sensitivity of ~a few mCrab (10^{-8} erg cm^{-2} s^{-1}). The BAT on-board software can autonomously detect and locate (within 10 s) GRB triggers with an accuracy of a few arcminutes and initiate autonomous slews pointing the narrow field instruments (XRT and UVOT) to the burst position on timescales of 100 s. The XRT detector is a JET-X Wolter 1 telescope with an E2V CCD-22 chip (as used in the EPIC camera on-board XMM-Newton), 600 × 600 pixels to a side, each 2.36 arcsec in size, yielding a FOV of 24 × 24 arcmin square. The XRT effective area is 110 cm^{-2} and is sensitive over the energy range 0.2–10 keV, peaking at 1.5 keV with a sensitivity of 1 mCrab in 10 ks. The angular resolution of XRT is 18 arcsec (HPD), with an energy resolution of ~140 eV at 5.9 keV (at launch). The UVOT is of a 30 cm, F12.7 modified Ritchey-Chrétien design and houses a CCD detector coupled to an image intensifier (micro-channel plate). This combination yields a high sensitivity (m_B = 24 in 1000 s in White light) over a large range in incident flux. UVOT houses 11 filters including optical U, B, V and ultraviolet UVW1,UVM2,UW2, as well as a White light filter, which together provide ≈1–1.5 arcsec imaging (depending on the filter) in several broad bands covering the range 1700–6000 Å over a field of view of 17 × 17 arcmin. Additionally UVOT has ultraviolet and optical grisms useful for slitless spectroscopic observations of bright sources.

One of the main science goals of *Swift* is the fast dissemination of GRB positions for dedicated ground and space-based follow-up. In this context, accuracy is of paramount importance,

particularly if prompt spectroscopic observations of bright, optical afterglows is desired.

As part of its routine service to the GRB science community, the BAT and XRT routinely provide, via the Gamma-Ray Burst Coordinates Network (GCN), automated on-board positions on timescales of less than a few minutes, and their respective science teams provide refined positions (after ground-based re-processing) on timescales of minutes–hours. For the majority of GRBs the XRT is the only narrow-field instrument on board *Swift* to provide a localised source position, that is, the majority of *Swift*-detected bursts are optically-faint, being either intrinsically faint, reddened, or at high redshift (see e.g. Roming et al. 2006), and are therefore below the detector sensitivity of the UVOT.

The XRT prompt positions have a precision of order 3.5 arcsec (systematic) with an additional statistical uncertainty based on the number of observed counts in the initial image (statistical error, $\epsilon = 22.63 \times \mathrm{counts}^{-0.48}$, see Hill et al. 2004). In the high-count regime, the majority of the uncertainty derives from the uncertainty in the attitude reconstruction provided by the star-trackers and uncertainties in the alignment of the boresight to the star-tracker (see e.g. Moretti et al. 2006). Conversely, for the UVOT, knowledge of the boresight and star-tracker solutions are of lesser importance, as, for any image with long enough exposure, UVOT images may be astrometrically corrected by matching positions of detected sources relative to those in stellar catalogues (e.g. USNO-B1) and applying an astrometric correction to the image. For a single UVOT image, the typical residual mean error in source positions, after applying astrometric corrections, is of order 0.5–1.0 arcsec, depending on the number and location of sources in the $17' \times 17'$ field of view of UVOT. Thus it is only for those rare occasions when there are insufficent stellar matches to provide an accurate astrometric solution, that knowledge of the UVOT boresight is essential.

By contrast our inability to provide accurate astrometric corrections to early XRT observations means that the uncertainty in the XRT positions places severe limitations on the ability of large aperture ground-based telescopes to perform early (within a few hours) spectroscopic observations of the GRB afterglow and its environment.

To improve this situation, we have undertaken an investigation to ascertain whether the UVOT can be used as a Super Star-Tracker, i.e. to provide the necessary aspect information to astrometrically correct XRT prompt positions, thereby providing GRB localisations with an accuracy and precision of better than a few arcseconds. This is particularly important if the GRBs are optically faint, and no obvious counterpart is seen in UVOT. Our investigation has a number of aims: (i) estimate the stability of the optical bench on which the XRT and UVOT are mounted, by determining within a single orbit, the accuracy with which XRT and UVOT track individual sources in detector coordinates, then if the tracking between XRT and UVOT proves sufficiently stable, (ii) determine an accurate mapping between XRT and UVOT detector coordinate systems, as a means of providing ultimately, (iii) XRT refined positions enhanced by UVOT astrometric solutions.

For step (i) we work in detector coordinates, and verify that drifts in source positions in detector coordinates within an orbit, caused by drift in the spacecraft attitude, are accurately tracked in both instruments. If this condition is satisfied, then in principal, XRT detector coordinates can be mapped into UVOT detector coordinates (step ii), transformed into the world coordinate system using the star-tracker solution, and then (step iii) aspect corrected with respect to a standard stellar catalogue.

Such a process is feasible, if and only if the following conditions are met:

- The pointing direction of the XRT and UVOT telescopes track each other with high precision (i.e. the flexure in the optical bench is minimal).
- Time-dependent focusing variations in both XRT and UVOT, due to changes in the mirror optics (for example, those caused by temperature variations) are minimal.
- There is sufficient temporal overlap between XRT PC mode and UVOT image mode data.

The paper is set out as follows: in Sect. 2, we investigate the accuracy with which XRT and UVOT track individual sources in detector coordinates. In Sects. 3 and 4 we outline a method for mapping XRT–UVOT detector coordinates. In Sect. 5 we describe in detail our implementation of an automated procedure for producing UVOT-enhanced XRT positions in real-time. In Sect. 6 we provide validation of our fitting procedure, and our list of UVOT-enhanced XRT positions for 148 GRBs. Finally, the results are summarised in Sect. 7.

2. Tracking the alignment between UVOT and XRT

In order to track the UVOT/XRT alignment during the course of an orbit, we have selected a target which has been observed in XRT PC event mode[1] and UVOT event mode, allowing us to time-slice the observations into short enough intervals to track any drift in the source position in detector coordinates, but with sufficient counts in the XRT to allow accurate centroiding on the source. We require that the XRT PC event mode data are not piled-up, i.e. sources with count rates of less than 0.6 ct/s. The bright, radio-loud AGN, 3C 279 ($m_{\mathrm{B}} = 17.8$), with an XRT (0.2–10 keV) count-rate of ∼0.3 ct/s is a suitable target for this analysis.

3C 279 has been observed on several occasions by *Swift* XRT as part of its routine calibration program. This analysis uses data taken between 2006-01-13T00:37:00 and 2006-01-13T23:37:57. With 14 orbits of usable data (15 ks XRT PC mode), the X-ray data was time-sliced into 100 s bins, providing 10 time slices per orbit, with approximately 30 ct/bin. For each time slice we extracted an image in detector coordinates and measured the source position by fitting the model PSF. The non piled-up PSF profile for an on-axis source at 1.5 keV can be modelled as a King function (Moretti et al. 2005) with coefficients $r_{\mathrm{c}} = 5.50$ and $\beta = 1.52$. We note that the background is negligible over a 100 s exposure. A sequence of 8 images each of 100 s duration is shown in Fig. 1, panels 1–8. Using the same time intervals we then accumulate images from the UVOT event list (Fig. 1, panels 9–16). Because UVOT event data are taken through several different filters (in this instance ≈3.8 ks in UVM2 and ≈5.9 ks in UVW2), this typically allowed 7–8 images to be constructed per orbit with overlapping XRT PC mode event data, half in UVW2 and half in UVM2. Figure 1 shows that in the first UVOT detector coordinate image, the source is significantly blurred. This blurring (which is present in detector coordinate images and not sky coordinate images), is also present in the first image of subsequent orbits, and is due to small residual movements in the spacecraft pointing direction immediately following the slew. The blurring is not present in sky coordinates because individual event positions are corrected for the

[1] While the XRT has a number of different observing modes, only Imaging and PC event mode data provide 2-dimensional images of the sky necessary for determining GRB positions.

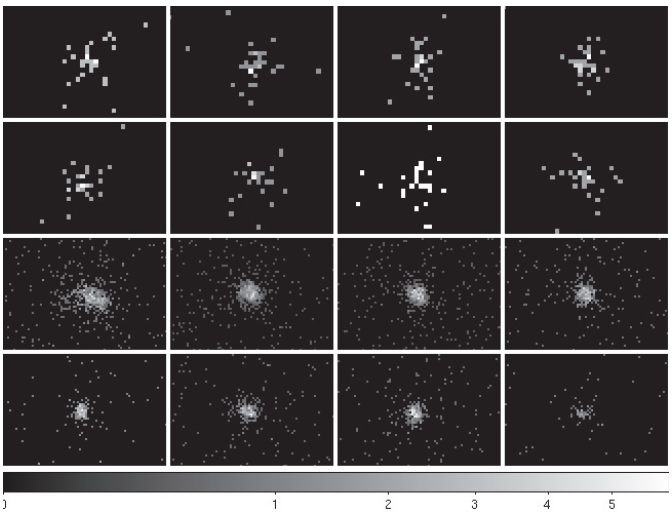

Fig. 1. *Top* – time-sliced (100 s) XRT PC mode detector coordinate images (82″ × 54″) for the first orbit of XRT PC mode data. *Bottom* – corresponding UVOT V-band detector coordinate images (4 in UVW2, followed by 4 in UVM2, each 40″ × 25″) spanning the same time intervals. Note the significant blurring of the source in the first panel of the UVOT data, is because the spacecraft is still in motion, and the events have been cast into a detector-coordinate image.

changing spacecraft attitude before being cast into an image. As a consequence large offsets in the UVOT (and also XRT) detector coordinate positions can be recorded between images taken during and after settling (see Fig. 2). We note that in some of the 3C 279 UVOT event mode data there is evidence for significant (>1.0″) changes in the detector coordinate position of an individual source due to filter changes within an orbit, though the occurrence of these is not easily predicted.

In Fig. 3 we show the detector coordinate positions for the XRT and the UVOT, for each of the 14 orbits of data (except orbit 13 which is unusable) (approximately 100 positions). The corresponding positions are highly correlated, particularly in the *y*-direction, for this particular roll angle (121.6 degrees). The *y*-directions for the XRT and UVOT detector coordinates are oriented 180+28.7 degrees relative to one another and are therefore expected to show a strong negative correlation in their detector dety coordinates, as is observed in Fig. 3.

The measured separation of the source position in detector coordinates between orbits 1 and 15 is 192.6 UVOT pixels and 39.4 XRT pixels respectively. For a pixel scale of 0.5 arcsec/pixel (UVOT) and 2.36 arcsec/pixel (XRT), this separation corresponds to 96.3 arcsec (UVOT) and 92.9 arcsec (XRT), i.e. a <4% error in the tracking (consistent with the accuracy to which the XRT pixel sizes are known). The difference in the angular direction is consistent with the optical bench design which has UVOT oriented 28.7 degrees relative to XRT along the *y*-axis, with their *y*-axes running in opposite directions.

The accuracy with which source positions are tracked in both detectors suggests that there is no evidence for flexure in the optical bench and that the azimuth for each of the two detector coordinate planes is aligned to very high precision.

3. Mapping XRT to UVOT detector coordinates

We start from the simplifying assumption that the detector plate scales for both instruments are linearised and both lie in the *x*-*y* plane. Any tilt in the azimuthal direction (i.e. the angle between the normals to the two detector planes) can manifest itself as a

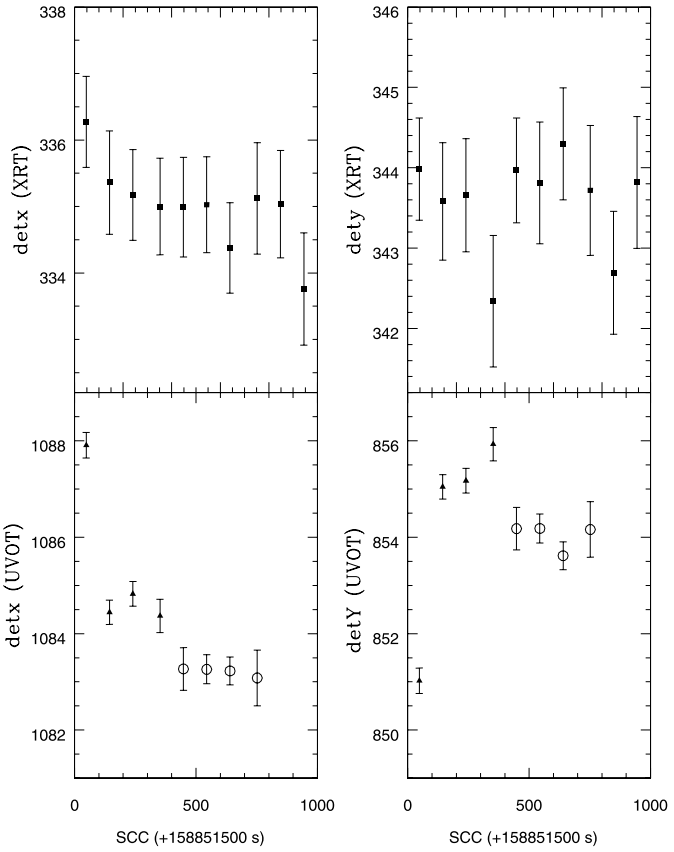

Fig. 2. A comparison of the detector coordinate positions of the XRT (*upper panels*) and the UVOT (*lower panels*) as a function of Space Craft Clock (SSC) time for one orbit of observations of 3C279. Filled squares XRT, filled triangles (UVOT – UVW2), open circles (UVOT – UVM2). One XRT pixel is 2.36 arcsec to a side. One UVOT pixel is 0.5 arcsec to a side.

change in the ratio of the plate-scales in both *x* and *y* directions. However we find no evidence for this. We fit the mapping between XRT and UVOT detector coordinates through a combination of rotation, zero-point offset, and multiplicative plate-scale (ratio of the size of UVOT to XRT detector pixels) by minimising the Δdetx, Δdety residuals between measured and predicted UVOT detector positions. That is, we minimise the difference between the predicted UVOT detector position ($U_{\mathrm{detx_p}}, U_{\mathrm{dety_p}}$) and the measured UVOT detector position ($U_{\mathrm{detx_m}}, U_{\mathrm{dety_m}}$) (determined by fitting the model PSF), where $U_{\mathrm{detx_p}}$, $U_{\mathrm{dety_p}}$ are given by:

$$\begin{pmatrix} U_{\mathrm{detx_p}} \\ U_{\mathrm{dety_p}} \end{pmatrix} = \alpha \begin{pmatrix} X_{\mathrm{detx}} \\ X_{\mathrm{dety}} \end{pmatrix} \begin{pmatrix} \cos\theta & -\sin\theta \\ \sin\theta & \cos\theta \end{pmatrix} + \begin{pmatrix} \delta \\ \epsilon \end{pmatrix} \quad (1)$$

where α is the ratio of the UVOT/XRT detector plate-scales, θ is the rotation angle between the two detectors, and (δ, ϵ) are the zero point offsets. Note that the form of this rotation matrix accounts for the ≈210 degree difference in orientation of the detector coordinate *y*-axes between XRT and UVOT.

Given the spacecraft pointing uncertainty (few arcminutes), the detector coordinate map relating XRT detector coordinate to UVOT coordinate positions must span a substantial fraction of the 17′ × 17′ field of view of UVOT. Thus we require a large number of observations covering a large fraction of the detector and spanning a large range in roll-angles (to reduce the likelihood of producing a map which is accurate along one direction only, since repeated pointings at similar roll angles tend to

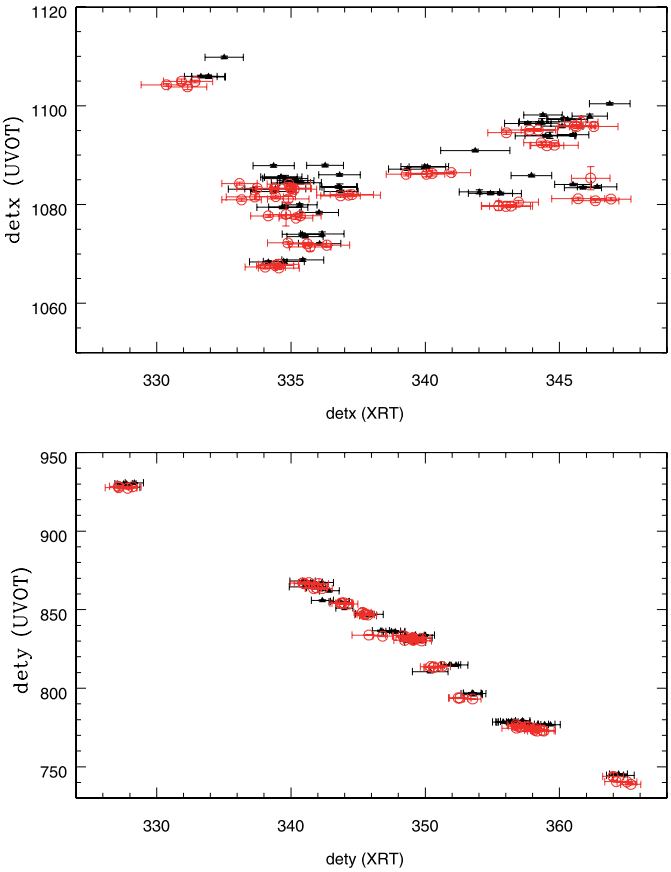

Fig. 3. Correlation between the detector coordinate positions of 3C 279 for XRT-PC and UVOT (UVW2 – black and UVM2 – red) event mode data. One XRT pixel is 2.36 arcsec to a side. One UVOT pixel is 0.5 arcsec to a side.

cover a very narrow area on the detector plane, and to verify that roll-angle effects are absent). The 3C 279 UVOT event mode data used previously to determine the tracking stability is unsuitable on its own due to the restricted range in roll-angles covered by these observations. Fortunately, there are numerous (>100) XRT PC-mode and UVOT V-band observations of 3C 279 taken over a large range in roll-angle and available within the public *Swift* data archive. The current (as of April 2006) UVOT filter wheel sequence for a new GRB is: 10 s V-band settling exposure, a 100 s White filter finding chart, 400 s V-band filter finding chart, followed by observations through all UV and optical filters in turn followed by a White filter and then V-band filter finding chart. We decided in the first instance to calibrate the map for the V-band filter only. White has not been used in the calibration as yet because although these observations begin once the as-settled flag is set, the spacecraft can still show large drifts in attitude (lasting up to a few hundred seconds after the GRB trigger), causing substantial drifts in the detector coordinate position. Since detector to sky coordinate conversions are determined for a specific instant in time, and GRBs generally fade rapidly (i.e. most of the X-ray photons arrive during the first few tens of seconds of the exposure) GRB X-ray detector coordinate positions can often be inaccurate if the spacecraft has not yet come to rest. For the majority of bursts V-band observations start when drifts in the spacecraft attitude are far smaller, so the V-band filter is the earliest to give an easily interpretable position.

Based on minimising the residuals between the predicted and measured UVOT positions in detector coordinates using observations of 3C 279 taken over a broad range in spacecraft roll angle and covering the central 8 arcmin of the XRT detector, the best-fitting model parameters are as follows: (θ = 28.7072, α = 4.69, δ = 481.72, ϵ = 3023.97) with a 90% confidence limit of 1.3″. Both the orientation, θ, and ratio of the plate-scale, α, are entirely consistent with the known relative detector geometries for XRT and UVOT.

4. PSF fitting of XRT PC-mode GRB prompt and early afterglow emission using the Cash-Statistic

Aside from the systematic error derived from the XRT-UVOT detector mapping, the precision with which a source position can be determined also depends upon the precision with which the XRT detector coordinate position can be determined, particularly in the low photon count regime when the statistical error on the XRT position will dominate the error budget.

In order to produce as accurate a position as possible, we have employed PSF fitting to determine GRB positions. The procedure is as follows: a list of potential sources in the XRT detector coordinate image is found using a specially written version of the *celldetect* algorithm (Harnden et al. 1984), which is tuned for the XRT PSF (Moretti et al. 2005), which at the same time is able to discount any potential residual hot-pixels as sources. For the exposures obtained during the UVOT/XRT data overlap intervals (see below), which are typically 100-400 s, the background level is negligible, and experience with the algorithm suggests a source can reliably be detected with as few as 10 counts with a S/N of 2.0. Once a source has been detected its position is determined using a PSF centroid fitting algorithm based on the maximum likelihood method of Cash (1979). The standard C-statistic from this paper is modified so that the integral of the PSF probability distribution is renormalised in the presence of bad CCD detector columns which have no exposure. Several such columns in the centre of the CCD resulted from a micrometeoroid strike on 2005 May 27 (Abbey et al. 2005).

The centroiding algorithm has been tested using Monte-Carlo simulations (see Fig. 4). Simulating sources with different numbers of counts, photons were drawn at random from the XRT PSF probability distribution and the centroid determined. Comparison of the distribution of position residuals obtained after 5000 simulations per run confirmed that the returned 90% statistical error, ϵ, derived from the fit for non piled-up data was accurate and followed the relation $\epsilon = 11.6$ counts$^{-0.5}$ arcsec.

We have also verified that the centroiding performs well in the presence of bad columns. At the time of writing, standard processing of XRT PC mode data removes 5 columns centred at detector x-coordinate 292 and 3 columns at 320. Simulations were performed as before, but either 3 or 5 columns were removed from the image at various offsets from the expected PSF centre. The results showed that the centroids were unaffected by the presence of 3 bad columns, while for 5 bad columns, a worse case residual offset of 0.6 arcsec was seen when the true source centre was placed inside the bad columns (Fig. 4). For comparison, a simple barycentre centroid estimator applied to the 5 bad column simulations showed a worse case offset of 2.4 arcsec. Based on these results, if a source centroid is found to be inside the 5 bad columns an additional systematic error of 0.6 arcsec is included. In Fig. 5 we show the XRT PC mode sky coordinate image from the first orbit of data for GRB 070419A,

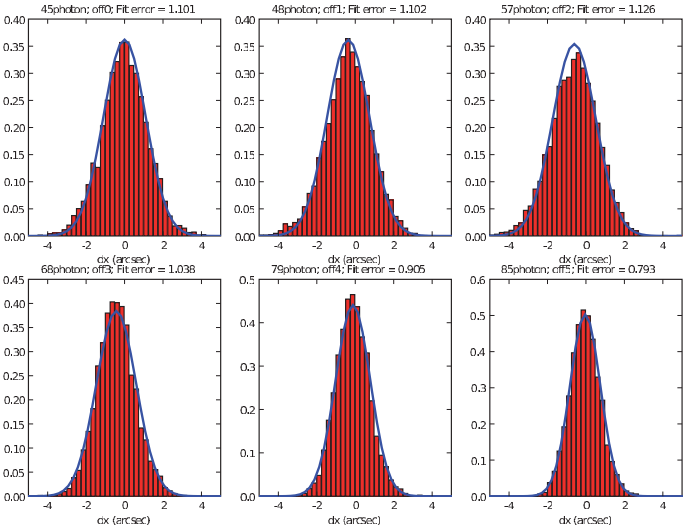

Fig. 4. Distribution of residuals obtained in simulations of XRT images when a non piled-up source is located near 5 bad columns. *From top-left to bottom-right*, the bad columns are systematically offset by, 0, 1, 2, 3, 4, 5 XRT pixels from the centre of the PSF. The red histograms show the distribution of differences of the simulated positions from the input position, while the blue curve is the Gaussian average fit error. The poorest case (a 2 pixel offset) yields a 0.6 arcsecond mismatch which is added as an additional systematic error when this offset occurs. There were 5000 simulations per run, for a source of 100 counts intensity.

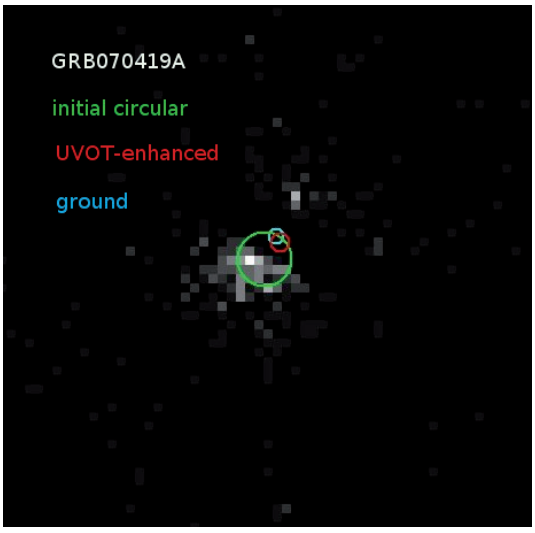

Fig. 5. A 2.2 × 2.2 arcmin sky coordinate image of the XRT PC-mode (1st orbit only) observations of GRB 070419A, a GRB which by chance is centred on the bad columns. Also shown are the XRT refined position (large circle) and the UVOT enhanced and ground-based optical positions, the small dark, and small light circles respectively). PSF fitting accounting for bad columns, provides improved position estimates and ultimately better final positions for XRT detected GRBs.

a burst which was severely affected by the presence of vetoed bad columns. Our UVOT-enhanced XRT position, using the PSF fitting routine, accounting for bad columns and the UVOT-XRT detector map, is a significant improvement on the XRT refined position (Stratta 2007).

During the XRT's automated response to a GRB, the observed X-ray light curve may be piled-up in Photon Counting mode when the observed count rate is greater than ∼0.6 count s^{-1} (see Vaughan et al. 2006). Because of this, we also tested how accurate the centroiding algorithm is when a source is piled-up. A

Table 1. King function PSF coefficients determined from piled-up sources used in the centroiding simulations.

Target/Obsid	Count rate[a]	r_c^b	β^c
3c273/00050900011	2.31	11.88	1.63
GK Per/00030842017	1.30	8.85	1.49
GK Per/00030842013	0.84	7.21	1.46

[a] Observed PC mode grade 0–12 count rate in a 30 pixel extraction circle. [b] Core radius (arcsec). [c] Index.

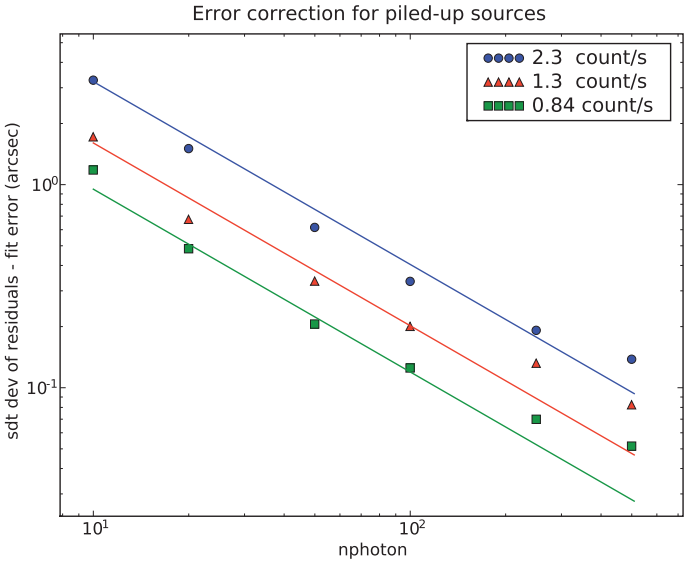

Fig. 6. The error correction term, ϵ, for simulated piled-up sources fitted with a non piled-up PSF. The solid lines represent the best fit parameterisation of the error correction curve (see text for details).

number of observations were selected from the *Swift* data archive which exhibit different levels of pile-up. For each observation a piled-up PSF profile was determined from the image. The coefficients describing the model piled-up PSF profiles (as fitted by a King function) are given in Table 1. The piled-up profile was used as the input PSF probability distribution for simulating sources, which then had their centroids fitted using the non piled-up PSF. The distribution of the residuals (i.e. the measured offset from the simulated position) is broader than the returned fit error if we use the non-piled up PSF to determine the position. That is, the distribution of residuals shows that the position statistical error, ϵ, is underestimated when the number of counts in an image is low and the data are piled-up. The simulations allowed a 90% confidence error correction term to be derived, to be added in quadrature to the formal fit error, equal to $15.3\,rate^{1.2} \times \mathrm{counts}^{-0.9}$, where *rate* is the observed count rate when greater than the non piled-up limit of 0.6 count s^{-1} (see Fig. 6).

5. Production of UVOT-enhanced XRT positions

The publicly available on-line quick-look data area is checked every 10 minutes for data associated with a new trigger number. Once a dataset containing both PC mode XRT data and *V*-band UVOT imaging data is made available by the *Swift* Data Center (SDC), the creation of a UVOT-enhanced XRT position is initiated. The process is fully automated. The timescale for which an enhanced position is produced depends ultimately on the timescale for which SDC processed down-linked data are delivered to the Data Centre Quick-Look area. In most cases

this will occur within a few hours of the burst trigger, unless the spacecraft is an orbit which does not pass over the Malindi ground station, during which time no data down-link is possible.

The automated position enhancement procedure works on the first observation of a new GRB, which is first broken down into times when PC mode X-ray data were obtained simultaneously with UVOT V-band images. Currently our automated procedure requires simultaneity of data since some drift in attitude is expected, particularly during the spacecraft settling phase. It is possible that this constraint may be relaxed in the future. In most cases[2] there will be at least one V-band image that overlaps with XRT-PC event mode data during the first orbit of observations (exceptions include: very bright bursts for which XRT remains in WT mode for the whole of the first orbit (e.g. GRB 051117A, Goad et al. 2007), delayed slews (which have a variety of causes, including Sun-Earth-Moon constraints), and bright stars in the UVOT field of view). Such times are referred to as *overlaps* throughout the rest of this paper. For each interval of overlap the following steps are taken:

- An XRT PC-mode detector co-ordinate image is produced from the cleaned event lists, and any sources therein are automatically detected. The position centroid of each detected source is determined using the PSF fitting routine described in Sect. 4. If no source is found within 40″ of the XRT TDRSS position (if available), or in cases where there is no XRT TDRSS position, within the 3 arcmin BAT error circle, this overlap is rejected.
  If an XRT TDRSS position is available, the source located closest to this position is assumed to be the GRB. Otherwise, for the first three overlaps the brightest source within the BAT position error circle is assumed to be the GRB. Experience shows that for prompt (within a few minutes) slews, the brightest source within the XRT field of view is the GRB afterglow. This is not necessarily true for delayed slews, or for XRT ToO observations of GRBs detected by other instruments. After this, the weighted mean of these three positions is calculated and the nearest source to this position is assumed to be the GRB.
- If the GRB position was determined using fewer than 10 XRT photons it is deemed unreliable and the overlap is rejected.
- If the source position is more than 40″ away from the XRT TDRSS position (when available) or from the weighted mean position (formed from the weighted average of UVOT enhanced XRT positions determined within each of the first three overlaps) of the UVOT-enhanced XRT position otherwise, it is flagged as a non-GRB and the overlap is rejected.
- The source position for the GRB in XRT detector coordinates is converted to an equivalent detector coordinate position for UVOT, using the XRT-UVOT detector coordinate mapping procedure described in Sect. 4. The UVOT detector position is then transformed into a sky coordinate position using the *Swift* tool SWIFTXFORM which applies the aspect information supplied by the star-trackers to the UVOT reference pixel.
- Serendipitous source positions in the UVOT sky coordinate image are matched with their corresponding optical counterparts in the USNO-B1 catalogue, using the *Swift* tool UVOTSKYCORR which determines the astrometric transformation required to correct UVOT sky-coordinate positions relative to USNO-B1. Overlaps containing UVOT astrometric corrections of >5″ resulting from drifts in the spacecraft attitude during the settling phase (which may last up to a few hundred seconds following a repointing of the telescope) are rejected as unreliable.
- Finally, the derived quaternions describing the transformation from the UVOT WCS to USNO-B1 WCS are applied to the XRT position, yielding for each overlap interval, an UVOT astrometrically-enhanced XRT position for the GRB.

The precision of the final position is formed from a combination of both statistical and systematic errors. These include the statistical uncertainty associated with the PSF fitting procedure (step 1), and the residual uncertainty in the astrometric solution relating UVOT WCS to USNO-B1 WCS (steps 5–6). These uncertainties are added in quadrature. From these we determine a weighted mean position and error. Any of the individual overlap positions which lie outside of the weighted means' 3-σ error circle are rejected as outliers and the weighted mean position and error re-calculated. Finally, the systematic uncertainty associated with the mapping between XRT–UVOT detector coordinates (1.3″, 90% confidence, Sect. 3) plus an additional systematic uncertainty, necessary to place 90% of optically detected GRBs within our 90% error circle (see Sect. 6), are added in quadrature at the end.

5.1. Dissemination of results

Once determined, the UVOT-enhanced XRT position is made available to the GRB community via an automated GCN circular. More detailed information is published electronically at `http://www.swift.ac.uk/xrt_positions`. This online material contains a list of every enhanced position produced, links to detailed results pages for individual bursts, and links to images of the UVOT filter sequence; as well as descriptions of the process of deriving these and other types of XRT position (e.g. SPER positions). The filter sequence images are a graphical representation of the UVOT observations through each filter and are provided both for completeness and diagnostic purposes.

The detailed results pages can be accessed by appending ⟨targetID[3]⟩/image.php to the above URL, and a page exists for each burst with at least one overlap. This page gives the source position and error, the number of overlaps included in the position determination and the total amount of exposure time within those overlaps. We also provide a breakdown of the number of overlaps excluded from the final position calculation and the reason for their rejection (i.e low counts, large astrometric correction etc.). These results are tabulated at the top of each page.

Below this, we provide two UVOT V-band images centred on the GRB position. The first image is a close up image from the summed, astrometrically corrected, UVOT V-band images overlaid with the enhanced XRT 90% confidence error circle. A larger version of this image is also provided, overlaid in this case with the position and error circle from each overlap. Those positions used to calculate the enhanced position are shown in green, positions rejected due to low counts are indicated in red, while all other rejected positions are in shown in yellow. Figure 7 shows one example, GRB 070318.

[2] At the time of writing, we have derived UVOT-enhanced XRT positions for 84 out of 120 GRBs detected by *Swift* since April 2006 when the current filter sequence was implemented, and for 148 bursts in total (see Table 2).

[3] The target ID is the trigger number padded to 8 digits with leading zeroes. e.g. GRB 070531 was trigger 280958, so has target ID 00280958.

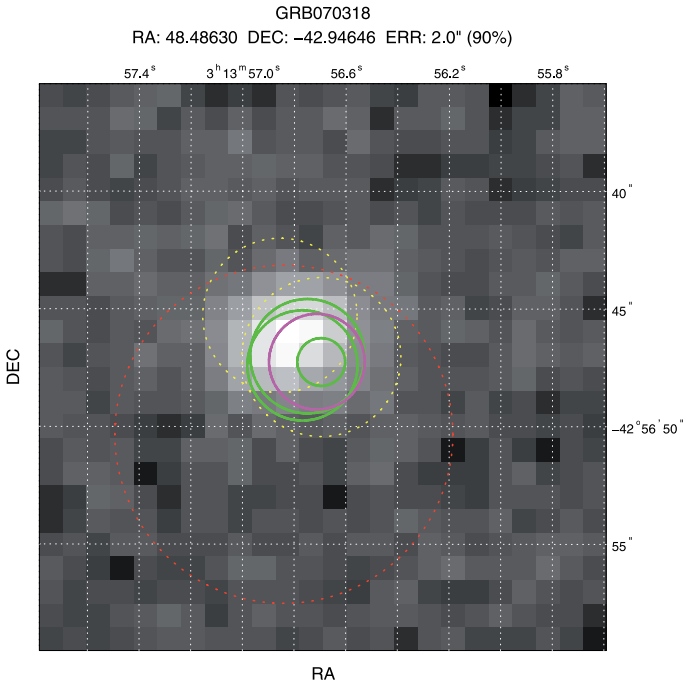

Fig. 7. An example 25x25 arcsecond UVOT sky coordinate *V*-band image from the detailed results page for GRB 070318 (see `http://www.swift.ac.uk/xrt_positions/00271019/image.php` for details). The final position (magenta) is based on 3 overlaps (green). One further overlap was rejected as the fit contains fewer than 10 photons (dashed red), and two were rejected as the astrometric correction was considered too large (dashed yellow).

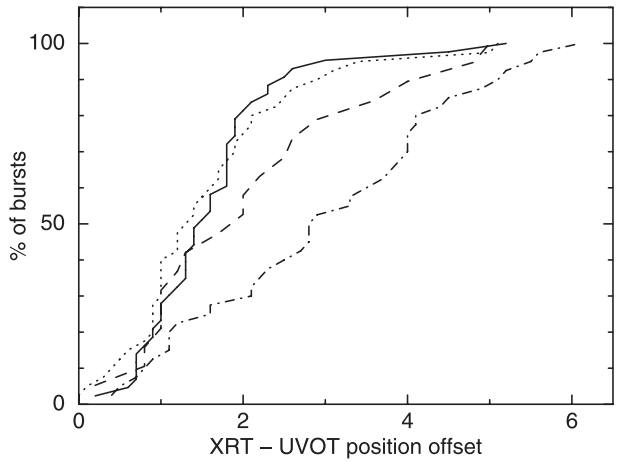

Fig. 8. The cumulative distribution of XRT position offsets (in arcseconds) with respect to 40 UVOT GRB positions available in the literature. Solid-line: UVOT-enhanced XRT position offsets, the result of this work. Dot-dashed line: "Refined" XRT position offsets, as derived in ground analysis and published in GCN circulars and the Swift data table at `http://swift.gsfc.nasa.gov/docs/swift/archive/grb_table/`. Dashed line: astrometrically corrected XRT positions at ≈24 h (Butler 2007). Dotted line: final astrometrically corrected positions from deep XRT images (Butler 2007).

5.2. When a position cannot be determined

An enhanced position cannot be determined for every burst. The most common reason for failure is the absence of overlapping PC-mode XRT data and *V*-band UVOT data. This can occur for example if the UVOT is in blocked mode, due to the presence of a bright star within the UVOT field of view. Alternatively, if the slew was delayed or the burst initially faint, the number of source counts at the location of the burst in XRT PC mode data may be less than the 10 counts required to reliably centroid on a source. Cases for which no position correction was possible are reported on the main results page. If at least one overlap exists, but no corrected position was produced, a detailed results page is also produced, and a brief explanation of the reason for the failure summarised on the main results page.

5.3. Manual intervention

The automated procedure is not a catch-all in that incorrect positions may in principle be made. For example, if the initial XRT GCN position notice is wrong, this could lead to an enhanced position for a non-GRB being produced. The same is possible if there is no XRT position notice and the brightest source in the BAT field of view at early times is not the GRB. Both of these eventualities are very unlikely, but not impossible. Such cases will be manually corrected. Furthermore, we have found at least two occurrences of incorrect attitude reconstruction for UVOT images of GRBs out of the many thousands of UVOT images of GRBs processed to date. In such cases the XRT team will supply an XRT refined position based on telemetered XRT PC-mode data, and a UVOT-enhanced XRT position from a manual application of the automated pipeline (using the refined XRT position as the starting position) as soon as the data allow.

6. Validation of results

In order to validate our procedure, we ran our automated position enhancement software pipeline for every GRB observed by Swift, yielding 148 enhanced positions up to GRB 070724A (i.e. enhanced positions for 60% of all bursts). Our success rate following the implementation of the latest UVOT filter sequence in April 2006 is ≈70% if we include only *Swift*-detected bursts. 40 of these GRBS were also detected by UVOT, for these we calculated the distance between the UVOT detected position and the UVOT-enhanced XRT position. Figure 8 shows the distribution of the offsets between our UVOT-enhanced XRT positions and UVOT detected positions obtained from the publicly available GCN notices for these 40 GRBs. 90% of the enhanced XRT positions fall within 2.5 arcsec of the UVOT detected position. We evaluated the uncertainty in the UVOT-enhanced XRT positions by comparing these positions' offsets from the UVOT positions divided by the errors of the UVOT-enhanced XRT and UVOT position errors added in quadrature.

Including the 1.3″ uncertainty in the XRT-UVOT mapping as the only systematic uncertainty we find that the position offset for 90% of the bursts is 1.25 times the combined error, suggesting that the systematic error is too small (Fig. 9, upper panel). Increasing the systematic error to 1.5″ ensures that the positions agree within the 90% errors, 90% of the time (Fig. 9, lower panel). At present the cause of the extra uncertainty is unknown, and the increase of our systematic error is a conservative move; it assumes that the quoted UVOT positions and uncertainties are accurate. In support of this claim, our own analysis of UVOT positions and uncertainties for GRB optical transients does not result in any additional systematic error component to that already found. It is possible that improved estimates for the UVOT detected source position and error may reduce the magnitude of this additional systematic uncertainty. However, this appears unlikely, given that UVOT position uncertainties are in

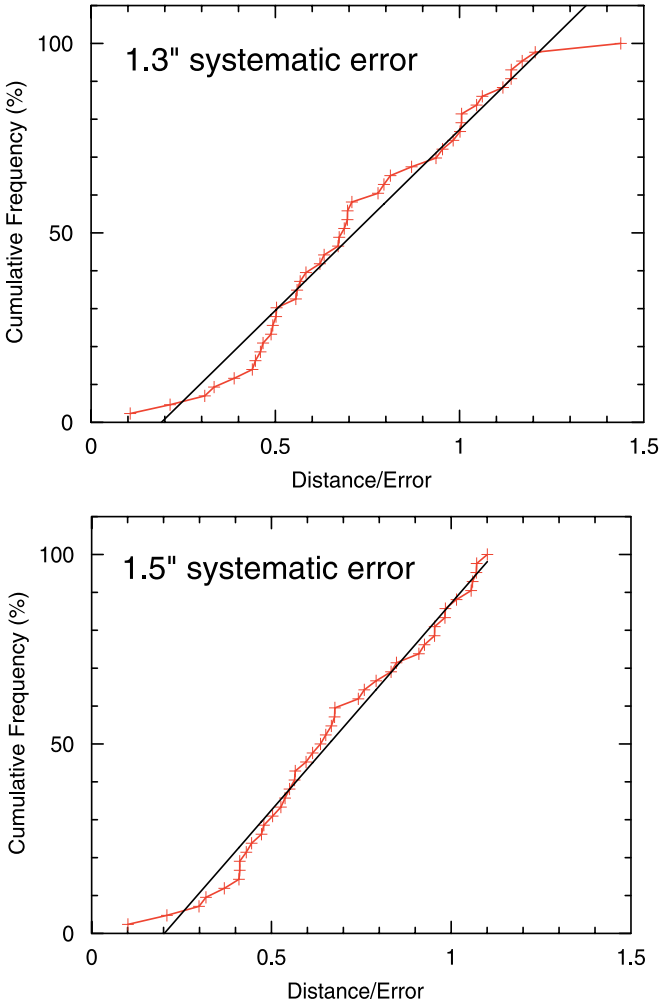

Fig. 9. Results of comparing the UVOT-enhanced XRT GRB positions with the UVOT GRB positions. The *upper panel* shows that when the 1.3″ systematic error derived from the UVOT-XRT mapping is included in the 90% error radius, the positions agree ∼80% of the time. After increasing the 1.3″ systematic to 1.5″ (*lower panel*), the positions agree 90% of the time.

the range 0.5–1.0″. Thus we suspect that the bulk of the additional systematic uncertainty in the UVOT-enhanced XRT positions must originate elsewhere. Additionally, as the number of OTs increases, improvements can be made to the UVOT *V*-band – XRT detector mapping (obviously, additional non-GRB pointings with simultaneous XRT PC mode and UVOT imaging data can also be used) .

Finally, while concerted effort has been made in determining an accurate map for the *V*-band filter, it is our intention to extend this process to other filters, particularly the White light filter which has the highest sensitivity and is used early in the filter sequence when the bursts are brighter.

The UVOT-enhanced XRT positions for 148 GRBs are shown in Table 2. 50% of the bursts have position errors below 2.1″; with the X-ray fainter bursts having larger errors, so that 90% of all bursts have position errors below 4.2″. The enhanced positions are automatically relayed to the Gamma Ray Burst community via GCN circulars, as well as being made available for public scrutiny on our web-pages located at `http://www.swift.ac.uk/xrt_positions`. An example UVOT *V*-band image with UVOT-enhanced XRT source positions overlaid is shown in Fig. 7.

Table 2. UVOT-enhanced XRT positions.

GRB Name	RA (J2000)	Dec (J2000)	Error† (″)
GRB 070724A	01 51 13.98	−18 35 39.8	2.2
GRB 070721B	02 12 32.84	−02 11 39.7	1.8
GRB 070721A	00 12 39.21	−28 33 00.7	2.2
GRB 070714B	03 51 22.29	+28 17 52.2	1.7
GRB 070714A	02 51 43.37	+30 14 36.2	1.9
GRB 070704	23 38 47.82	+66 15 11.8	2.7
GRB 070628	07 41 06.02	−20 16 45.6	1.6
GRB 070621	21 35 10.14	−24 49 03.3	1.7
GRB 070616	02 08 36.60	+56 56 43.8	2.3
GRB 070612B	17 26 54.48	−08 45 03.2	3.6
GRB 070610	19 55 09.61	+26 14 06.7	4.1
GRB 070531	00 26 58.48	+74 18 46.7	1.9
GRB 070521	16 10 38.57	+30 15 21.7	1.8
GRB 070520B	08 07 31.07	+57 36 28.9	2.5
GRB 070518	16 56 47.83	+55 17 43.0	2.2
GRB 070509	15 51 50.51	−78 39 07.1	2.5
GRB 070508	20 51 12.02	−78 23 05.0	2.0
GRB 070506	23 08 52.34	+10 43 20.3	2.9
GRB 070429A	19 50 48.91	−32 24 17.5	2.5
GRB 070420	08 04 55.13	−45 33 21.7	1.6
GRB 070419B	21 02 49.79	−31 15 48.5	1.6
GRB 070419A	12 10 58.83	+39 55 31.5	2.3
GRB 070412	12 06 10.11	+40 08 37.1	4.6
GRB 070411	07 09 19.78	+01 03 50.9	2.6
GRB 070328	04 20 27.60	−34 04 00.6	1.8
GRB 070318	03 13 56.69	−42 56 47.3	1.7
GRB 070311	05 50 08.21	+03 22 29.6	2.7
GRB 070306	09 52 23.25	+10 28 55.5	1.6
GRB 070224	11 56 06.65	−13 19 49.6	2.0
GRB 070220	02 19 06.86	+68 48 16.1	1.7
GRB 070219	17 20 45.91	+69 22 15.6	3.2
GRB 070208	13 11 32.76	+61 57 55.2	2.4
GRB 070129	02 28 00.89	+11 41 03.3	1.8
GRB 070110	00 03 39.30	−52 58 28.6	1.7
GRB 070107	10 37 36.49	−53 12 47.5	1.6
GRB 070103	23 30 13.74	+26 52 33.2	1.8
GRB 061222A	23 53 03.47	+46 31 57.6	1.6
GRB 061202	07 02 06.03	−74 41 54.4	1.7
GRB 061201	22 08 32.23	−74 34 49.1	1.7
GRB 061126	05 46 24.67	+64 12 40.0	1.6
GRB 061122	20 15 19.79	+15 31 02.3	2.0
GRB 061110A	22 25 09.81	−02 15 27.9	1.9
GRB 061021	09 40 36.17	−21 57 05.3	1.6
GRB 061019	06 06 30.92	+29 34 12.8	2.3
GRB 061007	03 05 19.70	−50 30 02.7	1.9
GRB 061006	07 24 07.88	−79 11 53.2	3.2
GRB 061004	06 31 10.80	−45 54 24.3	1.7
GRB 060929	17 32 28.93	+29 50 06.7	2.0
GRB 060927	21 58 12.01	+05 21 49.8	2.1
GRB 060926	17 35 43.75	+13 02 14.3	4.5
GRB 060923B	15 52 46.64	−30 54 14.7	2.5
GRB 060923A	16 58 28.12	+12 21 38.8	2.1
GRB 060919	18 27 41.76	−51 00 52.4	2.3
GRB 060912A	00 21 08.09	+20 58 19.1	1.7
GRB 060908	02 07 18.43	+00 20 32.8	1.6
GRB 060906	02 43 00.83	+30 21 42.6	2.1
GRB 060904B	03 52 50.57	−00 43 29.9	2.5
GRB 060814	14 45 21.34	+20 35 09.6	1.6
GRB 060813	07 27 35.33	−29 50 49.4	1.8
GRB 060807	16 50 02.62	+31 35 30.2	1.6
GRB 060805A	14 43 43.35	+12 35 12.3	2.8
GRB 060804	07 28 49.27	−27 12 56.1	1.7
GRB 060801	14 12 01.32	+16 58 54.4	1.9
GRB 060729	06 21 31.81	−62 22 12.1	1.7
GRB 060719	01 13 43.72	−48 22 50.9	1.9

Table 2. continued.

GRB Name	RA (J2000)	Dec (J2000)	Error (″)
GRB 060714	15 11 26.45	−06 33 59.3	1.7
GRB 060708	00 31 13.72	−33 45 34.1	1.9
GRB 060707	23 48 19.11	−17 54 17.6	1.7
GRB 060614	21 23 32.06	−53 01 36.2	1.9
GRB 060607A	21 58 50.46	−22 29 47.3	1.6
GRB 060605	21 28 37.32	−06 03 30.7	1.7
GRB 060604	22 28 55.36	−10 54 55.4	5.2
GRB 060526	15 31 18.31	+00 17 06.2	1.8
GRB 060522	21 31 44.86	+02 53 10.1	1.8
GRB 060512	13 03 05.70	+41 11 26.5	1.9
GRB 060510B	15 56 29.37	+78 34 11.6	2.0
GRB 060507	05 59 50.41	+75 14 56.0	2.6
GRB 060502B	18 35 44.79	+52 37 55.7	6.3
GRB 060502A	16 03 42.58	+66 36 01.5	1.8
GRB 060428B	15 41 25.77	+62 01 29.8	2.4
GRB 060428A	08 14 10.77	−37 10 11.7	1.7
GRB 060427	08 17 04.29	+62 40 17.0	2.3
GRB 060418	15 45 42.70	−03 38 21.0	2.0
GRB 060413	19 25 07.82	+13 45 30.1	1.6
GRB 060319	11 45 32.91	+60 00 39.2	2.0
GRB 060313	04 26 28.41	−10 50 41.2	2.0
GRB 060306	02 44 22.74	−02 08 55.1	3.5
GRB 060223A	03 40 49.50	−17 07 48.7	4.2
GRB 060218	03 21 39.65	+16 52 01.0	2.1
GRB 060211A	03 53 32.70	+21 29 19.2	4.1
GRB 060210	03 50 57.31	+27 01 33.8	1.6
GRB 060206	13 31 43.51	+35 03 02.0	2.7
GRB 060204B	14 07 15.05	+27 40 36.9	2.0
GRB 060203	06 54 04.00	+71 48 39.3	3.5
GRB 060202	02 23 22.92	+38 23 03.6	1.8
GRB 060123	11 58 47.75	+45 30 51.4	4.4
GRB 060121	09 09 52.14	+45 39 47.7	2.4
GRB 060116	05 38 46.24	−05 26 13.9	3.0
GRB 060115	03 36 08.27	+17 20 41.8	2.5
GRB 060111B	19 05 42.55	+70 22 32.2	2.2
GRB 060111A	18 24 49.22	+37 36 15.7	4.6
GRB 060109	18 50 43.65	+31 59 27.2	2.3
GRB 060105	19 50 00.74	+46 20 56.6	1.7
GRB 051221A	21 54 48.24	+16 53 22.7	3.6
GRB 051211B	23 02 41.13	+55 04 48.8	2.5
GRB 051109B	23 01 50.29	+38 40 47.2	2.3
GRB 051109A	22 01 15.30	+40 49 22.7	1.7
GRB 051028	01 48 14.99	+47 45 10.0	4.2
GRB 051021A	01 56 36.25	+09 04 01.0	2.2
GRB 051016B	08 48 27.97	+13 39 19.7	2.4
GRB 051016A	08 11 16.93	−18 17 55.4	4.3
GRB 051008	13 31 29.45	+42 05 52.7	2.0
GRB 050922C	21 09 32.97	−08 45 30.6	1.7
GRB 050922B	00 23 13.68	−05 36 17.0	2.6
GRB 050922A	18 04 21.99	−32 10 51.1	4.6
GRB 050918	17 51 12.14	−25 34 39.0	3.3
GRB 050915A	05 26 45.14	−28 01 01.1	2.8
GRB 050908	01 21 50.92	−12 57 17.8	4.6
GRB 050904	00 54 51.13	+14 05 06.0	1.9
GRB 050827	04 17 09.59	+18 12 02.0	2.6
GRB 050826	05 51 01.65	−02 38 34.9	4.7
GRB 050822	03 24 27.37	−46 02 00.8	2.2
GRB 050820A	22 29 38.12	+19 33 37.1	1.8
GRB 050819	23 55 01.53	+24 51 41.2	3.5
GRB 050815	19 34 22.98	+09 08 46.6	5.1
GRB 050814	17 36 45.30	+46 20 21.6	2.1
GRB 050803	23 22 37.91	+05 47 09.4	1.7
GRB 050802	14 37 05.80	+27 47 11.5	2.3
GRB 050730	14 08 17.21	−03 46 19.3	1.6
GRB 050724	16 24 44.07	−27 32 26.5	2.9
GRB 050717	14 17 24.49	−50 32 00.8	2.3
GRB 050716	22 34 20.40	+38 41 07.0	3.7
GRB 050714B	11 18 47.66	−15 32 48.4	3.6
GRB 050713A	21 22 09.34	+77 04 29.6	1.8
GRB 050712	05 10 48.29	+64 54 48.6	2.4
GRB 050603	02 39 56.96	−25 10 54.2	1.7
GRB 050509C	12 52 21.03	−44 26 00.9	2.5
GRB 050505	09 27 03.30	+30 16 23.8	1.6
GRB 050504	13 24 01.29	+40 42 14.7	3.6
GRB 050502B	09 30 10.13	+16 59 47.5	1.9
GRB 050416A	12 33 54.55	+21 03 27.0	1.9
GRB 050408	12 02 17.31	+10 51 09.5	2.1
GRB 050319	10 16 47.93	+43 32 55.3	1.8
GRB 050318	03 18 50.95	−46 23 44.7	2.2
GRB 050315	20 25 54.07	−42 36 01.5	2.0
GRB 050306	18 49 14.58	−09 09 06.9	5.3
GRB 050219B	05 25 16.02	−57 45 27.8	2.8
GRB 050124	12 51 30.70	+13 02 41.3	4.7

† All errors 90% confidence radius.

7. Summary

We have constructed an automated pipeline for producing *Swift* XRT positions enhanced by UVOT astrometry, which are made available within a few hours of a GRB trigger. Our position determinations have not only increased precision (≈a factor of 2 reduction in error radius) relative to the refined XRT positions previously in use, but additionally have an accuracy relative to optically localised positions which is a factor of 2 better than the previous refined XRT positions. The positional accuracy obtained using this technique is superior to astrometrically corrected X-ray positions (obtained by matching X-ray sources to optical counterparts) at early times (for up to 24 h), and is comparable to the accuracy achieved using this technique at later times.

References

Abbey, et al. 2005, in The X-ray Universe 2005, ESA-SP 604, 943
Barthelmy, S. D. 2004, Proc. SPIE, 5165, 175
Barthelmy, S. D., Barbier, L. M., Cummings, J. R., et al. 2005, Sp. Sc. Rev., 120, 143
Burrows, D. N., Hill, J. E., Nousek, J. A., et al. 2004, SPIE, 5165, 201
Burrows, D. N., Hill, J. E., Nousek, J. A., et al. 2005, Sp. Sc. Rev., 120, 165
Butler, N. R. 2007, AJ, 133, 1027
Cash, W. 1979, ApJ, 228, 939
Gehrels, N., Chincarini, G. Giommi, P., et al. 2004, ApJ, 611, 1005
Goad, M. R., Page, K. L., Godet, O., Beardmore, A., & Osborne, J. P. 2007, A&A, 468, 103
Harnden, F. R., Fabricant, D. G., Harris, D. E., & Schwartz, J. 1984, SAO Rep. 393
Hill, J. E., Burrows, D. N., Nousek, J. A., et al. 2004, SPIE, 5165, 217
Moretti, A., Campana, S., Mineo, T., et al. 2005, SPIE, 5898, 360
Moretti, A., Perri, M., Capalbi, M., et al. 2006, A&A, 444, L9
Roming, P. W. A., Kennedy, T. E., Mason, K. O., et al. 2005, Sp. Sc. Rev., 120, 95
Roming, P. W. A., Schady, P., Fox, D. B., et al. 2006, ApJ, 652, 1416
Stratta, G. 2007, GCN Circ., 6323
Vaughan, S., Goad, M. R., Beardmore, A. P., et al. 2006, ApJ, 638, 920